Downloaded from rsta.royalsocietypublishing.org

PHILOSOPHICAL TRANSACTIONS OF THE ROYAL SOCIETY A MATHEMATICAL, PHYSICAL & ENGINEERING SCIENCES

The Breakdown of Superfluidity in Liquid ^{4}He VI. Macroscopic Quantum Tunnelling by Vortices in Isotopically Pure He II

P. C. Hendry, N. S. Lawson, P. V. E. McClintock, C. D. H. Williams and R. M. Bowley

Phil. Trans. R. Soc. Lond. A 1990 **332**, 387-414
doi: 10.1098/rsta.1990.0122

Email alerting service Receive free email alerts when new articles cite this article - sign up in the box at the top right-hand corner of the article or click **here**

To subscribe to *Phil. Trans. R. Soc. Lond. A* go to: **http://rsta.royalsocietypublishing.org/subscriptions**

This journal is © 1990 The Royal Society

Downloaded from rsta.royalsocietypublishing.org

MATHEMATICAL, PHYSICAL & ENGINEERING SCIENCES
THE ROYAL SOCIETY A
PHILOSOPHICAL TRANSACTIONS OF

The breakdown of superfluidity in liquid ^{4}He VI. Macroscopic quantum tunnelling by vortices in isotopically pure He II

By P. C. Hendry[1], N. S. Lawson[1], P. V. E. McClintock[1], C. D. H. Williams[1]† and R. M. Bowley[2]

[1] *Department of Physics, University of Lancaster, Lancaster LA1 4YB, U.K.*
[2] *Department of Physics, The University, Nottingham NG7 2RD, U.K.*

Contents

1. Introduction 388
2. Experimental details 389
3. Experimental results 391
4. Discussion 394
   (*a*) Analysis of 12 bar data 396
   (*b*) Analysis of data at higher pressures 397
   (*c*) Fitting the theory to the data 399
   (*d*) Electric field dependence of the tunnelling rate 405
   (*e*) The cross section for phonon-driven vortex nucleation 410
5. Conclusion 412
   References 413

Measurements are reported of the rate ν at which negative ions nucleate quantized vortices in isotopically pure superfluid ^{4}He for electric fields E, temperatures T and pressures P within the range $10^3 \leqslant E \leqslant 10^6$ V m^{-1}, $75 \leqslant T \leqslant 500$ mK, $12 \leqslant P \leqslant 23$ bar (= 2.3 MPa). The form of $\nu(E, T)$ differs in unexpected ways from that observed in earlier work at higher P, exhibiting: a pronounced dip in $\nu(T)$ at *ca.* 0.3 K whose depth and precise position depends on E and P; an exponential increase in $\nu(T)$ at higher T, with an activation energy considerably smaller than the roton energy gap; and distinct structure in $\nu(E)$. The experimental data are discussed and analysed in terms of the macroscopic quantum tunnelling model proposed by Muirhead *et al.* (*Phil. Trans. R. Soc. Lond.* A **311**, 433 (1984)). The relatively small barrier heights of *ca.* 2–3 K deduced from the data on this basis are construed as confirmation that the initial vortex is a loop rather than an encircling ring. The temperature dependence of ν at low pressures is interpreted in terms of a phonon-driven vortex nucleation mechanism, and values for its cross section are extracted from the data. The minima in $\nu(T)$ are ascribed to phonon damping of the tunnelling process, and the kinks observed in some of the low-temperature $\nu(E)$ curves are attributed to tunnelling of the system into the first excited state of the nascent vortex loop.

† Present address: Department of Physics, University of Exeter, Exeter EX4 4QL, U.K.

Phil. Trans. R. Soc. Lond. A (1990) **332**, 387–414 *Printed in Great Britain*

The Royal Society is collaborating with JSTOR to digitize, preserve, and extend access to *Philosophical Transactions: Physical Sciences and Engineering.* www.jstor.org

Downloaded from rsta.royalsocietypublishing.org

1. Introduction

Studies of the motion of negative ions constitute the only sure method by which the breakdown of the superfluidity of He II through the creation of quantized vortices may be investigated. In contrast, the onset of dissipation in bulk flow, or normal fluid/superfluid counterflow (Tough 1982), usually seems to relate to the expansion of vorticity pre-existing (Awschalom & Schwarz 1984) in the liquid, rather than to the *creation* of vortices. There is some possibility that the intrinsic creation process may, however, have been observed in experiments on flow through microscopic orifices (Hess 1971; Avenel & Varoquaux 1985; Varoquaux *et al.* 1986; Beeken & Zimmermann 1987); but the situation remains rather ambiguous (Schwarz 1987; Avenel & Varoquaux 1987).

Even in the case of negative ions, useful physical information about the vortex creation process can be acquired only under special conditions. This is because of the need for some method of limiting the ionic velocity which, otherwise, in the absence of dissipation, would increase continuously for any finite electric field. In practice the result would be an uncontrolled and almost immediate production of a charged vortex ring by each ion, too rapidly for the details of the physical mechanism to be discerned. In common with earlier work on vortex creation, described in the third paper in this series on the breakdown of superfluidity (Bowley *et al.* 1983, hereafter referred to as III), the present research uses roton creation above the Landau critical velocity v_L as a means of controlling the speed of the ions: thus the force due to the electric field is balanced by the rate of momentum loss corresponding to the production of rotons. For the technique to work it is obvious that the critical velocity v_c for vortex creation must exceed v_L; this situation can be brought about by the application of external pressure $P \gtrsim 10$ bar† to the liquid (Rayfield 1966). The use of the technique brings with it the disadvantage that the ion is in a continuous state of acceleration and it also relies on the assumption that roton emission and vortex creation are independent processes. We return to discuss these points in more detail below. For investigation of vortex creation in ^{4}He, it is also necessary that the sample should have been isotopically purified (Hendry & McClintock 1987) to remove the *ca.* 1.7×10^{-7} parts of ^{3}He found in naturally occurring gas-well helium. Otherwise, as discussed in detail in the fourth paper of the series (Nancolas *et al.* 1985, hereafter referred to as IV) the vortex creation rate is markedly increased, even by this very small proportion of ^{3}He isotopic impurity, and its dependences both on electric field and on temperature are profoundly modified.

The other earlier papers in this series on the breakdown of superfluidity in ^{4}He are the following: Allum *et al.* (1977), hereafter referred to as I, describing an experimental test of Landau's explanation of superfluidity; Ellis *et al.* (1980), hereafter referred to as II, on excitation emission from ions travelling at extreme supercritical velocities; and Ellis & McClintock (1985), hereafter referred to as V, reporting and discussing a precise experimental determination of the Landau critical velocity for roton creation.

The present paper describes an extension of the research of III to lower pressures. That is, it reports and discusses measurements of the vortex nucleation rate ν in isotopically pure ^{4}He in the pressure range down to 12 bar which was inaccessible in the earlier work. To prevent ν from becoming too large to measure in this régime

† 1 bar = 10^5 Pa.

Downloaded from rsta.royalsocietypublishing.org

where $(v_c - v_L)$ becomes small, it was necessary to use weaker electric fields than in III; this, in turn, necessitated an extension of the experiments to lower temperatures to be able to reach the temperature-independent régime where the vortex creation process is unaffected by the thermal excitations of the liquid. Some new and quite unexpected phenomena have been observed: as discussed below, they constitute a valuable contribution to our understanding of the mechanism of vortex nucleation. In particular, these new results appear to provide strong support for the general picture proposed by Muirhead *et al.* (1984), in terms of a macroscopic quantum tunnelling model: in what follows below, we refer to their paper as MVD.

In the next section we outline the experimental arrangements and, in particular, we describe how these differed from those already reported in detail in III. In §3 we present the main experimental results. In §4 these are discussed and analysed in some detail, mostly in terms of the MVD model. Finally, in §5, we summarize the main conclusions arising from the work and list the principal questions still remaining unanswered.

2. Experimental details

The investigations employed the same dilution refrigerator, cryogenics, isotopically pure ^{4}He, gas-handling arrangements and experimental cell that have already been described in detail in V. For the present work, however, the electrode structure inside the cell was radically modified so as to provide a collector geometry similar to that of III. Thus, as discussed in the latter paper, it was possible to deduce the vortex nucleation rate ν from the exponentially decaying signal induced in the collector by a group of approaching ions. The final version of the three electrode geometries used is sketched in figure 1.

In the earlier nucleation work (III) it was found that the signals became too small to be useful at pressures below 17 bar for the low-temperature limit, and at pressures below 19 bar when the temperature was raised sufficiently for the thermally activated vortex nucleation process to become significant. To extend the work to lower pressures, it was therefore essential to enhance the signal:noise ratio before averaging. This was accomplished in three ways. First, the cell used was much larger than that used in III. The diaphragm that determined the area of the ion cloud was of radius 25 mm, as compared to 6.8 mm in III, thus increasing the area and (for a given charge density) the induction current by a factor of 14.

Secondly, the sequence of voltages applied to the field emission ion sources was entirely different to that used in III: it was suspected that much of the signal attenuation at low pressures in the latter case was caused by vortex nucleation in the high-field region near the emission tips. The arrangement used in the present case was similar to that described in V. That is, a very brief negative voltage pulse of *ca.* 1.5 kV is applied to the tip; this is followed by a period during which the tips are held at a weak negative potential relative to the gate grid, to assist ions in penetrating the gate; and, as soon as the ions have been gated, the tips are made positive with respect to the gate so that they can help to re-absorb any bare ions or charged vorticity remaining within the emission region.

Finally, the signal:noise was enhanced directly by provision of an active (driven) guard around the collector lead. The latter was the centre conductor of a triaxial cable formed from a length of 48 s.w.g enamelled Eureka wire, inside a $\frac{1}{2}$ mm cupronickel capillary tube (the guard), in turn screened by a length of 2 mm cupronickel tubing from which it was insulated by a PTFE sleeve. With this

Downloaded from rsta.royalsocietypublishing.org

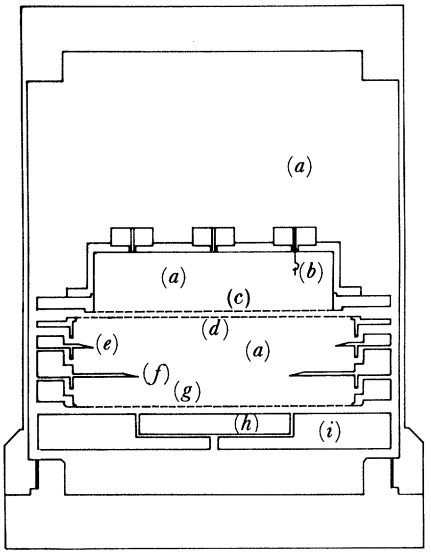

Figure 1. Sketch (not a section) of the experimental cell, showing the disposition of the electrodes for the nominally 1.92 mm length induction space: (*a*) liquid helium sample; (*b*) one of the seven field emission ion sources; (*c*) first gate grid; (*d*) second gate grid; (*e*) field homogenizing electrode; (*f*) diaphragm to define diameter of charge disk; (*g*) grid at high end of induction space; (*h*) collector; (*i*) driven guard electrode for collector. The region of high electric field, in which the measurements of ν are made, lies between (*g*) and (*h*). Further details of the cell construction are given in V.

arrangement, the total capacitance shunting the amplifier input circuit was reduced to about 12 pF. A 47 kΩ measuring resistor could then be used, compared to 5 kΩ without the active guard, yielding a correspondingly larger signal for the same rise time. The guard system inevitably introduced some additional noise, so that the final signal:noise enhancement factor was about 2.5.

Three lengths of induction space were used to investigate nucleation in different pressure and voltage ranges, of nominally: 11.3 mm; 3.90 mm and 1.92 mm. One of the electrode arrangements is shown schematically in figure 1. The length at room temperature in each case was determined to an accuracy of *ca.* ±2% by direct measurement. During data analysis small adjustments were made (see §4*d* below) to give agreement between velocities deduced from the induction signals and the much more accurate velocities previously measured in V for the same values of P, E and T. The geometry of the induction space was such that nonlinear terms in the expression for the signal in the absence of vortex nucleation events (see III) were negligible. In the worst case (the 11.3 mm cell, $\nu \approx 200\ \mathrm{s}^{-1}$) the error in ν from this cause, as deduced directly from the exponent of the decaying induction signal, would have been 3%. For most of the data it would have been very much smaller than this: the typical error of 0.05% is very much smaller than the random scatter in the data.

During data acquisition, the system was triggered, usually at a repeat frequency of 16 Hz, at a fixed point in the phase of the mains supply. The fixed point could be adjusted so as to avoid mains-synchronous 'glitches' which otherwise could give rise to systematic errors in the results. To remove spurious transients caused by the high voltage pulses to the emission tips, a method of systematic noise reduction was used in which the signals on alternate triggers were subtracted from the average, and the

Downloaded from rsta.royalsocietypublishing.org

gate was opened only on the other triggers. Thus the true signal repetition rate was usually 8 Hz. The number of signals in each average varied between 1000 and 40000, depending on the raw signal:noise in the parameter range being investigated.

The method used for extracting values of nucleation rate and velocity from the averaged data, by fitting curves to cursor-selected regions of the signal, was as previously described in III. It was established that the measured values of ν were independent of the signal repetition rate, though some overall warming of the cell was detectable at high rates. In practice, the cell temperature was stabilized, by means of a standard feedback circuit, the variations being limited to about ± 1 mK below $T = 350$ mK, and to about ± 5 mK at higher temperatures where the operation of the dilution refrigerator tended to become erratic.

3. Experimental results

In this section we present a representative sample of the experimental results, and comment briefly on them; detailed discussion and analysis is given in §4.

Data were recorded within the pressure, temperature and electric field ranges of $12 \leqslant P \leqslant 23$ bar, $75 \leqslant T \leqslant 500$ mK, $10^3 \leqslant E \leqslant 10^6$ V m^{-1}. Within this large parameter space it was obviously necessary to be selective. The majority of the data was recorded at pressures of 13, 15, 17.25, 19 and 21 bar, using the 11.3 and 3.90 mm cells. The lowest pressure used was 12 bar and, although some useful results were obtained in the 3.90 mm cell at this pressure, the signal:noise was relatively poor and the time needed to acquire the data was disproportionately long. A few data were recorded in the 3.90 mm cell at $E = 293$ kV m^{-1} for $P = 21$ and 23 bar, to confirm that the measured values of ν agreed with those of III. The 1.92 mm cell was used to extend the measurement of ν up to $E = 1$ MV m^{-1} at $P = 13$, 14, 15, 16, 17.25, 18, 19 and 21 bar.

Most of the results were taken in the form of sets of $\nu(T)$ measurements at fixed values of E, and a series of such sets of data, plotted against reciprocal temperature, is shown in figure 2*a–j*. It is immediately evident that most of these results differ in interesting ways from the $\nu(T^{-1})$ plots at higher pressure presented in III. First, the temperature at which the rapid increase in ν takes place has shifted down from *ca.* 0.6 K at 25 bar to *ca.* 0.2 K at 12 bar (figure 2*a*). Secondly, a number of the curves (figures 2*d–j*) display distinct local minima near 0.3 K. This effect was not noticed originally in the data reported in III, but can in fact be seen in some of the results if they are inspected carefully.

The data (circles) in figure 2*i* and *j* are compared with the results of III (triangles) recorded at the same electric field. The agreement is seen to be satisfactory; which is reassuring considering that the two sets of data were taken quite independently at different times, in different cryostats, using cells of quite different dimensions, with different samples of purified ^{4}He and using different thermometers, pressure gauges and other instrumentation.

Sets of $\nu(E)$ data were also recorded at fixed values of P and T. Most of these were in the low-temperature limit ($T < 140$ mK) where ν is independent of T (see figure 2*a–j*). A set of such results is shown in figure 3, where the pressure (bars) is given in each case by the number associated with the data points in question. An interesting feature of these results is the change in slope that occurs at intermediate electric fields; it is also evident that the position of the maximum in $\nu(E)$ falls towards lower E with increasing pressure and then increases again. Some possible reasons for the

Downloaded from rsta.royalsocietypublishing.org

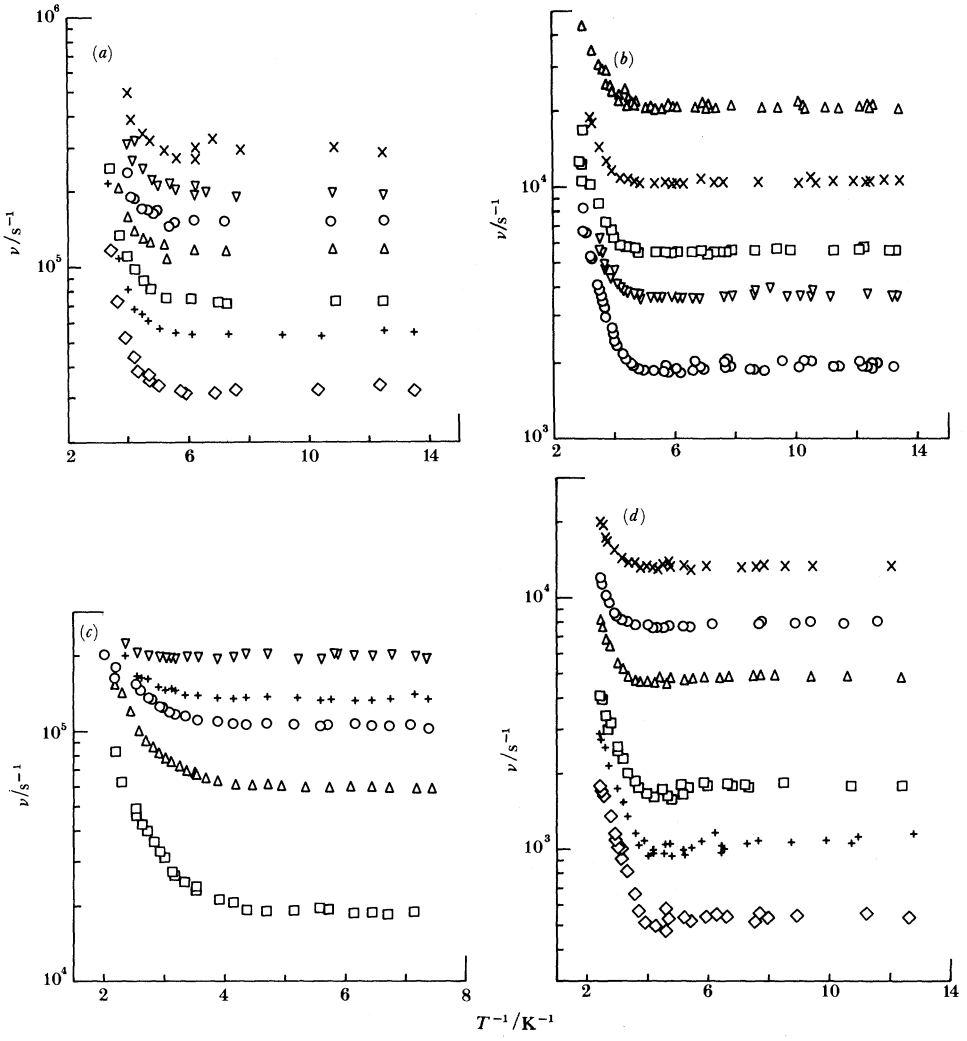

Figure 2. Plots of the measured vortex nucleation rate ν as a function of reciprocal temperature T^{-1} for various pressures P and electric fields E, as indicated below. Note that the abscissa scales are not all the same. (*a*) $P = 12$ bar and: $E = 8.85$ (◇); 13.3 (+); 17.7 (□); 31.0 (△); 44.2 (○); 62.0 (▽); 80.0 (×) kV m^{-1}. (*b*) $P = 13$ bar and: $E = 8.83$ (○); 13.3 (▽); 17.7 (□) 31.0 (×); 1000 (△) kV m^{-1}. (*c*) $P = 14$ bar and: $E = 100$ (□); 200 (△); 300 (○); 500 (+); 1000 (▽) kV m^{-1}. (*d*) $P = 15$ bar and: $E = 8.85$ (◇); 13.3 (+); 17.7 (□); 31.0 (△); 44.2 (○); 80.0 (×) kV m^{-1}. (*e*) $P = 16$ bar and: $E = 30.0$ (◇); 50.0 (▽); 70.0 (□); 100 (△); 300 (+); 500 (×); 1000 (○) kV m^{-1}. (*f*) $P = 17.25$ bar and: $E = 8.85$ (◇); 13.3 (▽); 17.7 (□); 31.0 (△); 44.0 (+); 62.0 (○); 80.0 (×) kV m^{-1}. (*g*) $P = 18$ bar and: $E = 100$ (▽); 300 (□); 500 (×); 1000 (○) kV m^{-1}. (*h*) $P = 19$ bar and: $E = 31.0$ (▽); 44.2 (□); 62.0 (△); 80.0 (+); 97.3 (○); 135 (×) kV m^{-1}. (*i*) $P = 21$ bar and: $E = 293$ kV m^{-1} present data (○) compared with measurements reported in III (▽). (*j*) $P = 23$ bar and: $E = 293$ kV m^{-1} present data (○) compared with measurements reported in III (▽).

decrease in ν in very strong E were mentioned in III, and we return to the problem again below, but most of the present discussion is in fact devoted to the relatively low field region where this particular complicating factor can be ignored.

Concurrently with the measurements of $\nu(P, E, T)$, the ionic drift velocity $\bar{v}(P, E, T)$ was also determined from the same induction signals (see III). The only

Downloaded from rsta.royalsocietypublishing.org

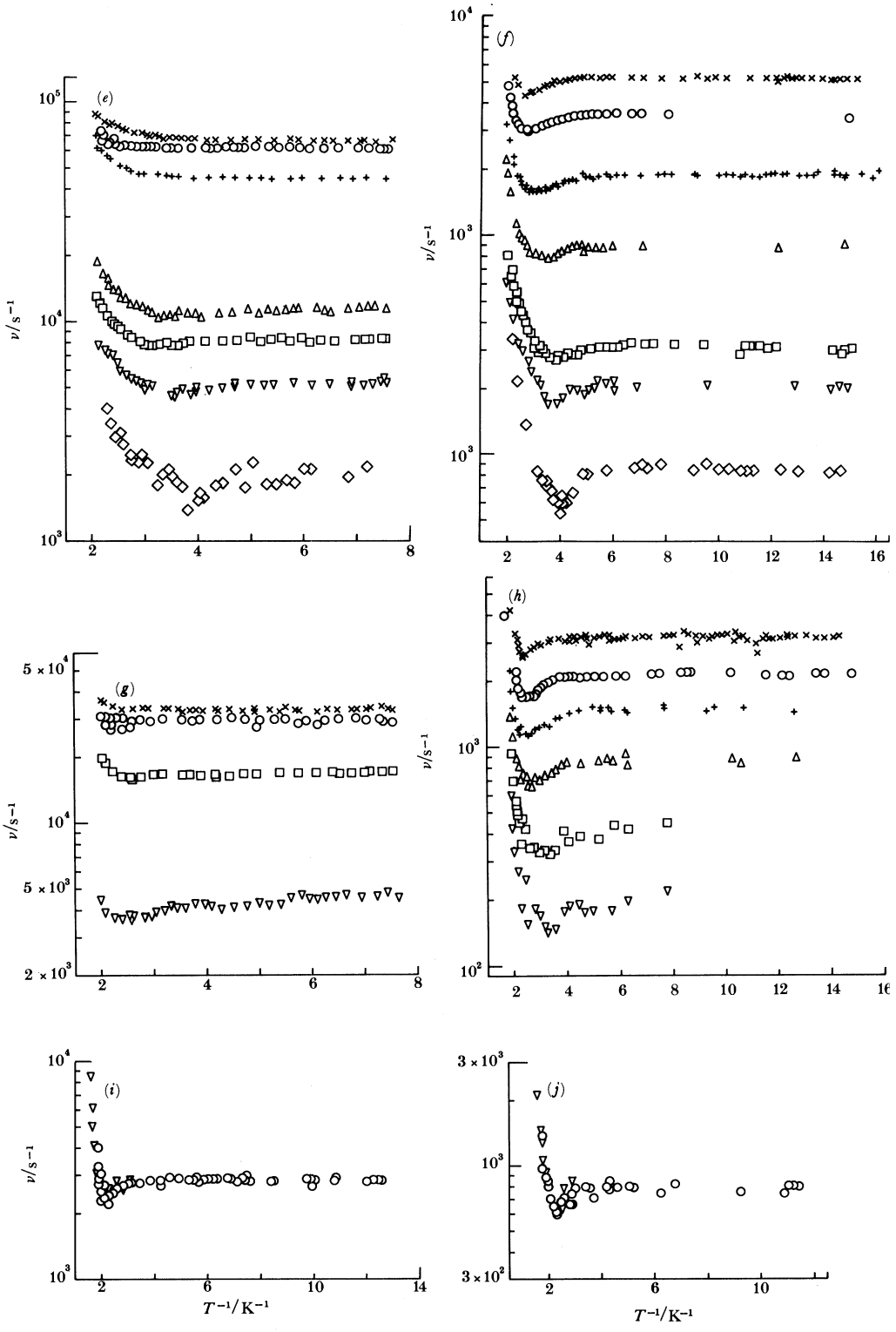

Figure 2*e–j*. For description see opposite.

Downloaded from rsta.royalsocietypublishing.org

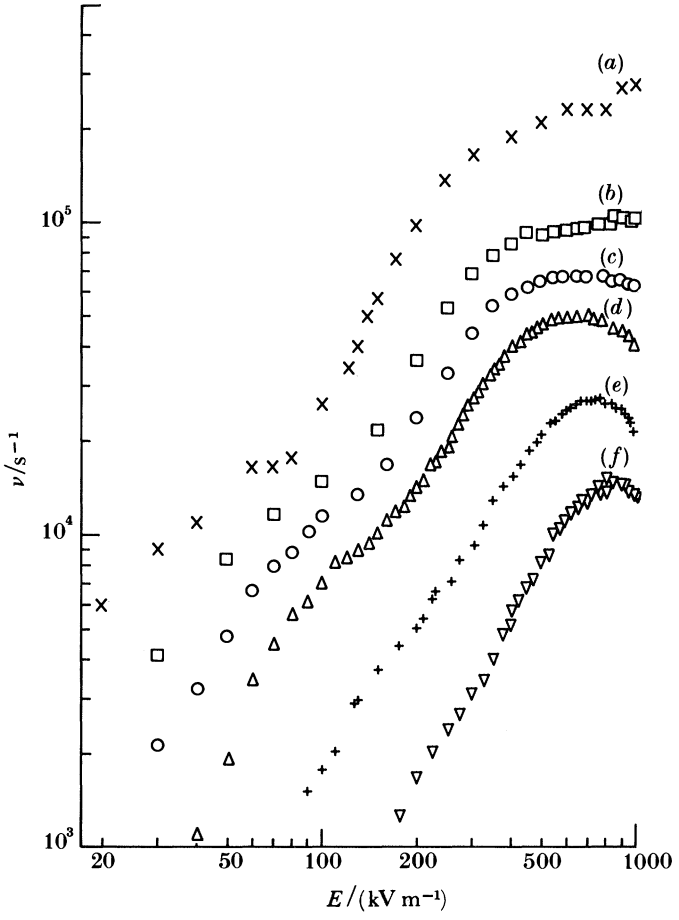

Figure 3. Measurements of the vortex nucleation rate ν in the temperature-independent régime below 140 mK plotted as a function of electric field E for the pressures (in bars) indicated by the letters above the data-sets: (*a*) 13; (*b*) 15; (*c*) 16; (*d*) 17.25; (*e*) 19; (*f*) 21.

exceptions were where ν was so large that almost all the ions created vortex rings before reaching the collector and the trailing edges of the corresponding induction signals were insufficiently well defined to allow satisfactory measurements of $\bar{v}$. Over most of the parameter range covered by the experiments, $\bar{v}$ was temperature independent within experimental error: only at the highest temperatures was the density of the excitation gas sufficient to reduce the velocity to a measurable extent. Some representative $\bar{v}(T)$ velocity data are plotted in figure 4*a* and *b*.

4. Discussion

The results reported in the preceding section differ in two important respects from those reported in III. First, there are the pronounced minima in some of $\nu(T^{-1})$ plots although as discussed above, evidence for their presence can also be seen in some of the earlier data. Secondly, although not immediately obvious by inspection of the figures, the exponential increase of ν at high temperatures no longer corresponds, at

Downloaded from rsta.royalsocietypublishing.org

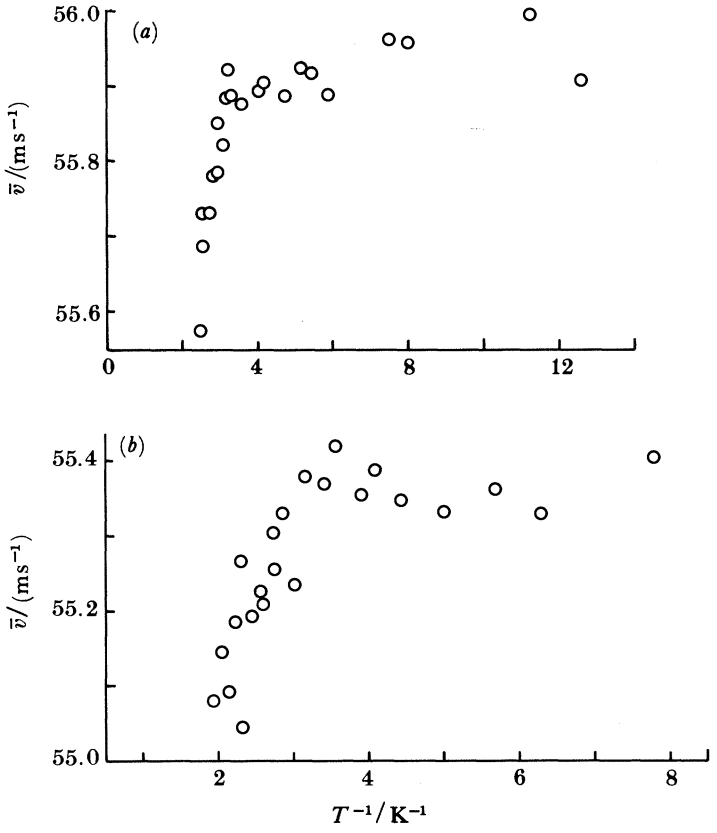

Figure 4. Examples of ionic drift velocities as measured from electric induction signals, plotted as functions of reciprocal temperatures, T^{-1}, for different pressures, P, and electric fields, E: (*a*) for $P = 15$ bar, $E = 8.85$ kV m^{-1}; (*b*) for $P = 19$ bar, $E = 31.0$ kV m^{-1}.

these lower pressures, to an exponent equal to Δ/kT where Δ is the roton energy gap. Rather, the exponent is $-E_b/kT$, where $E_b \leqslant \Delta$.

In this section, we analyse and discuss the experimental data in the context of the MVD model. In §4*a* we analyse some of the data at 12 bar where there is no minimum in $\nu(T^{-1})$ and we extract a value of the energy barrier E_b that impedes formation of the vortex. We discuss the $\nu(T^{-1})$ minima in §4*b* and propose that they may plausibly be accounted for in terms of a phonon damping mechanism affecting the tunnelling process, although alternative explanations are also possible. In the light of the ideas developed in §4*a* and *b*, we fit the theory to the full pressure range of $\nu(P, E, T)$ data in §4*c* and discuss the results. In §4*d* we discuss the structure seen in the experimental $\nu(E)$ curves at low temperatures and we propose that it can be understood, at least in part, in terms of tunnelling into excited states of the nascent vortex; we also extract from the data values of the vortex core parameter a, the critical velocities v_{v1}, v_{v2}, the instantaneous vortex nucleation rate constant R, and hence the characteristic tunnelling frequency ω_0. The unexpectedly strong electric field dependence of the cross section for the phonon-assisted nucleation process is discussed in §4*e*.

Downloaded from rsta.royalsocietypublishing.org

In what follows it must be constantly be borne in mind that, rather than moving at a uniform velocity, which would be the ideal case, the ion is continually accelerating. This means, in terms of the MVD model, that the tunnelling or thermal activation processes take place through or over a barrier that is shrinking. We implicitly assume that the vortex nucleation processes can reasonably be discussed in terms of the *average* velocities and barrier heights at which they occur. To do otherwise, and take explicit account of the moving barrier, would be extremely difficult because the necessary theoretical tools have yet to be developed. We believe, however, that discussion in terms of average quantities is valuable in that it affords physical insight into the nucleation mechanism even though it is unlikely to yield results that are quantitatively accurate.

(*a*) *Analysis of 12* bar *data*

The data recorded at a pressure of 12 bar for fixed electric fields (figure 2*a*) can be fitted by the equation:

$$\nu(T) = \nu_0 + AT\exp(-E_b/k_B T). \tag{4.1}$$

The term ν_0 describes a temperature-independent nucleation process which we believe (Hendry *et al.* 1987, 1988) corresponds to tunnelling of the vortex from the ion. The second term involves thermal activation over a potential barrier of height E_b. The prefactor AT arises, as we shall see, from the assumption that the process involves interaction with a single phonon of sufficient energy, kicking the system over the barrier. Other temperature dependences (including temperature independence) of the prefactor would also be consistent with the experimental results, and would lead to slightly differing values of E_b when fitted to the data. Using AT as the prefactor, we obtain $E_b/k_B = 2.4$ K for all the electric fields used at 12 bar. Comparisons of some of the data and fitted curves are shown in figure 5.

This value of E_b is a surprisingly small energy. It implies that the initial vortex must itself be very small and, at most, a loop of radius a few ångströms†. We can conclude immediately, therefore, that this activation process does not involve the creation of large encircling rings as proposed previously by Pines (1966), Schwarz & Jang (1973) and Bowley (1984). The present data thus constitute strong evidence in favour of the vortex loop model analysed in detail by MVD. These authors showed that the energetically most favourable configuration of the emergent vortex loop is on the 'equator' of the ion, where the 'north pole' is in its direction of motion and the plane of the loop points 'north'. MVD consider the loop to be a segment of a circle, so that the only parameter needed to describe it is its radius R. They estimated the radius to be about 5 Å at 17.5 bar, with a corresponding critical velocity of 57 m s^{-1} (see fig. 8*c* of MVD).

Thermal activation processes in He II involve either rotons (dominant above *ca.* 0.6 K) or phonons. The 12 bar data show evidence of thermal activation well below 0.4 K where the number of rotons in the liquid is negligible. The process in question must therefore involve phonons.

A phonon of energy larger than E_b can in principle kick the ion so as to produce a vortex. More precisely, interaction with a phonon of wave vector $\boldsymbol{k}$ can lead to the creation of a vortex loop on the ion if the phonon energy is larger than $E_b + \hbar\boldsymbol{k}\cdot\boldsymbol{v}$ where $\boldsymbol{v}$ is the velocity of the ion. The sound velocity c is much larger than $|\boldsymbol{v}|$ so, to

† 1 Å = 10^{-10} m.

Downloaded from rsta.royalsocietypublishing.org

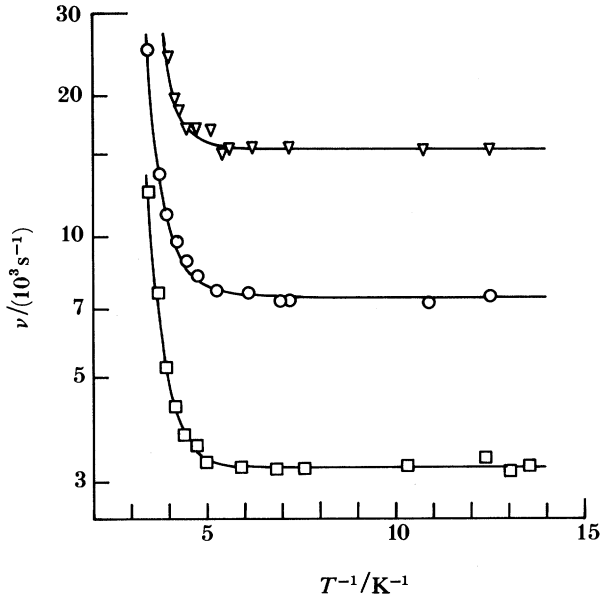

Figure 5. Comparison of equation (4.1) with experimental data at 12 bar. The measured vortex nucleation rates ν (points) are plotted as a function of reciprocal; temperature T^{-1} for three electric fields: □, 8.85×10^3 V m^{-1}; ○, 1.77×10^4 V m^{-1}; ▽, 4.40×10^4 V m^{-1}. The curves represent (4.1) with $E_b/k_B = 2.4$ K.

order v/c, we can ignore the $\hbar\boldsymbol{k}\cdot\boldsymbol{v}$ term. When averaged over angles, this procedure will give rise to an error of order v^2/c^2.

We suppose that interactions with phonons in the requisite energy range cause vortices to form on the ion at a rate $cn_p\sigma$ where σ is the cross section for the process and the number density n_p of phonons of energy larger than E_b is given by:

$$n_p = \frac{1}{2\pi^2}\int_{E_b/\hbar c}^{\infty} \mathrm{d}k k^2 \exp(-\hbar ck/k_B T)$$

$$\approx \frac{k_B T E_b^2}{2\pi^2\hbar^3c^3}\exp(-E_b/k_B T). \tag{4.2}$$

If we assume that σ is a constant, independent of phonon energy, then we obtain the thermal activation term of equation (4.1) with the prefactor AT where

$$A = \sigma k_B E_b^2/2\pi^2\hbar^3c^2. \tag{4.3}$$

From fitting (4.1) to the 12 bar data (figure 5) we find that $A = (1.2\pm0.1)\times10^8$ s^{-1} at this pressure. Using the sound velocity (Brooks & Donnelly 1977) of $c = 312$ m s^{-1}, we find $\sigma = 2$ Å. This result represents a plausible cross section for a process involving a vortex loop of the size envisaged.

(*b*) *Analysis of data at higher pressures*

The simple model described by (4.1) clearly cannot be used to fit the data recorded at pressures of 15 bar and above because of the minima in $\nu(T)$. As shown in figure 2*c–j* the minimum, which is barely visible at 15 bar, has become quite pronounced at 17 and 19 bar. The minima were unexpected before the experiments, but their existence appears to imply that the tunnelling term $\nu_0(E,T)$ in (4.1) decreases with

Downloaded from rsta.royalsocietypublishing.org

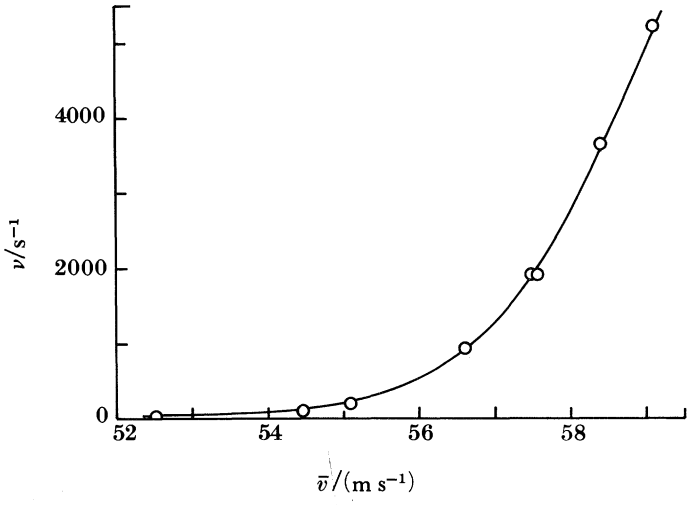

Figure 6. The vortex nucleation rate ν in the low-temperature limit ($T \leqslant 100$ mK) at 17 bar, plotted as a function of the ionic drift velocity $\bar{v}$. The smooth curve is a guide to the eye.

increasing temperature. We can suggest two simple reasons why such an effect might occur, and we now consider each of them in turn.

First, it is possible that the increase with temperature of phonon scattering from the ion could reduce its velocity sufficiently to cause the observed reduction in ν. This idea can be tested (Hendry *et al.* 1989) by analysis of the measured values of $\bar{v}(E, T)$. From the known variations of $\nu_0(E)$ with E at very low T (below 100 mK), we can obtain an estimate of the reduction in ionic velocity that would be needed to cause the observed dips in $\nu(T)$; this can then be compared with the measured values of $\bar{v}(T)$. The simplest way to carry out this procedure in practice is to plot $\nu(E)$ directly against $\bar{v}(E)$ for $T < 100$ mK, as shown in figure 6. Reading off values of $\bar{v}$ necessary to cause the dip in $\nu(T)$ shown for 17 bar in figure 7*a* then results in the small filled circles of figure 7*b*, which are to be compared with the actual velocity measurements shown by the open circles in the same figure. It is clear that the observed variation of $\bar{v}(T)$ is too small, by almost an order of magnitude, to account for the dip in $\nu(T)$, effectively disapproving the hypothesis. The only way in which this first explanation of the dip in $\nu(T)$ could still conceivably be valid would require there to be a very strong velocity dependence of the ion–phonon scattering cross section, such that the high-velocity tail of the distribution function could be strongly attenuated without significant effect on the average ionic velocity $\bar{v}$; there is no evidence to support such a scenario, and we do not regard it as probable.

There is a second, quite different, mechanism through which phonons could effect the tunnelling rate of vortices. Phonon scattering off the vortex loop as it tunnels could reduce the tunnelling rate by the factor (Caldeira & Leggett 1983) $\exp(-\phi\eta D^2)$, where η is a dissipation coefficient, D is the distance the vortex must tunnel through the barrier and ϕ is a numerical factor. The idea that dissipation might affect the tunnelling rate was considered by MVD: in particular, they argued that roton *emission* at a rate τ_r^{-1} could decrease the vortex nucleation rate by a factor $\exp(-\phi m d D^2/\hbar\tau_r)$ where md is the mass of a vortex loop of length d. Here, we are proposing that the phonon *scattering* rate τ_{ph}^{-1} should be included as well. Unlike the roton emission rate, which to an excellent approximation depends only on electric

Downloaded from rsta.royalsocietypublishing.org

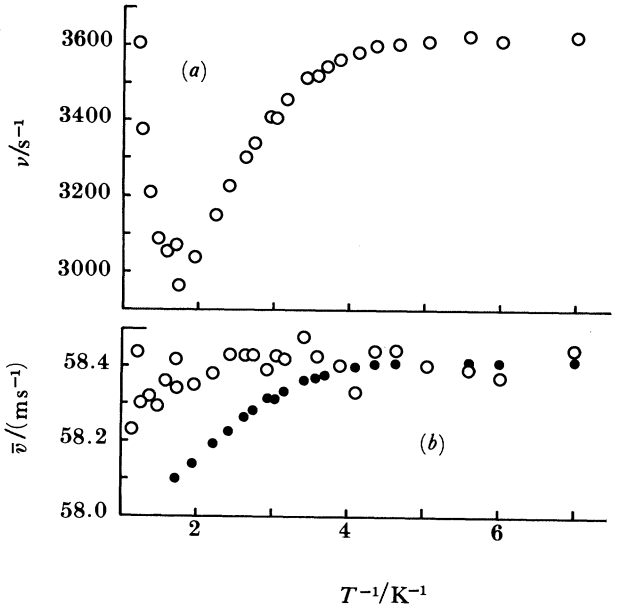

Figure 7. (*a*) The vortex nucleation rate ν at 17 bar as a function of reciprocal temperature T^{-1}, plotted with an expanded ordinate scale to emphasize the minimum in $\nu(T^{-1})$. (*b*) The corresponding drift velocities $\bar{v}$ measured from the same set of induction signals (open circles). The small filled circles represent the values of $\bar{v}$ that would be needed to generate the observed dip in $\nu(T^{-1})$.

field in the temperature range being considered, τ_{ph} depends not only on the cross section (Fetter 1964) but also on the thermal phonon density: it will consequently be strongly temperature dependent and could therefore give rise to the dips observed in $\nu(T)$.

For simplicity, we may take η to vary as T^3, like the phonon number density, in which case we would expect the nucleation rate to be described by

$$\nu(T) = \nu_0 \exp(-BT^3) + AT \exp(-E_{\mathrm{b}}/k_{\mathrm{B}}T) \tag{4.4}$$

in place of (4.1). The quantities E_{b} and B should be almost independent of applied electric field, but may be expected to vary smoothly with pressure. The relation (4.4) is found in practice to provide a satisfactory description of $\nu(T)$ at the higher pressures and so, in the interests of consistency, we have fitted it to the full pressure range of $\nu(T)$ data shown in figure 2.

(*c*) *Fitting the theory to the data*

At 12 bar the quality of the fit is, of course, fairly insensitive to the value of B: the data can be fitted almost equally well with $B = 0$ or $B = 3$. This can be understood in terms of the constant A being relatively large at 12 bar, so that the thermally activated region occurs at a sufficiently low temperature that it effectively masks the effect of the damping factor $\exp(-BT^3)$ with the consequence that no dip is seen. As the pressure increases, A decreases, the effect of the damping factor becomes relatively more pronounced, and the dip then appears.

The procedure adopted in practice to obtain a self-consistent fit of equation (4.4) to the data has been to fit the results at high pressure first. In this region, more accurate values of B could be obtained. Weighted averages of the fitted values of B

Downloaded from rsta.royalsocietypublishing.org

Table 1. *Values of parameters obtained by fitting equation* (4.4) *to* $\nu(T)$ *data measured at constant pressures and electric fields*

(The quoted errors represent the statistical uncertainties in the fitting procedure. Because the errors are correlated, the values are sometimes quoted to a greater precision than appears to be justified, in order to give sets of parameters that provide a good fit to the measurements.)

$E/(\mathrm{kV\ m^{-1}})$	ν_0/s^{-1}	$A/10^6$	$(E_b/k_B)/\mathrm{K}$	B
		$P = 12$ bar		
8.80	3240 ± 60	100 ± 50	2.365 ± 0.12	3.2
13.3	9250 ± 300	111 ± 90	2.21 ± 0.25	3.2
17.7	7370 ± 300	113 ± 90	2.21 ± 0.25	3.2
31.0	11700 ± 300	124 ± 180	2.19 ± 0.40	3.2
44.0	15700 ± 300	5000 ± 12000	3.0 ± 0.5	3.2
62.0	20700 ± 600	2800 ± 9000	2.783 ± 0.8	3.2
80.0	30740 ± 1000	209 ± 90	2.0 ± 1	3.2
		$P = 13$ bar		
8.80	1866 ± 30	5.3 ± 0.9	1.86 ± 0.05	3.7
44.0	13520 ± 60	8.67 ± 0.25	1.64 ± 0.06	3.7
80.0	20800 ± 250	18.5 ± 1	1.76 ± 0.15	3.7
		$P = 15$ bar		
8.80	505 ± 30	0.056 ± 0.020	1.14 ± 0.14	4.5
13.1	1020 ± 25	0.130 ± 0.036	1.30 ± 0.11	4.5
17.7	1790 ± 25	0.44 ± 0.15	1.67 ± 0.13	4.5
31.0	4860 ± 30	1.03 ± 0.20	1.84 ± 0.08	4.5
44.0	8055 ± 31	1.48 ± 0.22	1.88 ± 0.06	4.5
62.0	11300 ± 120	0.510 ± 0.160	1.33 ± 0.13	4.5
		$P = 16$ bar		
30.0	2000 ± 130	0.42 ± 0.65	1.83 ± 0.70	6.9 ± 8.5
50.0	5910 ± 80	0.27 ± 0.14	1.41 ± 0.24	9.7 ± 2.4
70.0	8490 ± 64	1.04 ± 0.35	1.99 ± 0.19	4.2 ± 1.0
100	11560 ± 130	1.15 ± 0.46	1.86 ± 0.23	4.2 ± 1.6
300	45200 ± 230	2.07 ± 0.88	1.88 ± 0.26	0.3 ± 0.7
500	67700 ± 360	0.88 ± 0.19	1.41 ± 0.22	0.33 ± 0.95
1000	62600 ± 900	0.36 ± 0.64	1.40 ± 1.6	0.31 ± 2.9
		$P = 17$ bar		
8.80	88 ± 2	0.13 ± 0.73	2.28 ± 0.25	21 ± 5
13.3	189 ± 8	1.3 ± 3.7	3.95 ± 1.6	−6 ± 2
17.7	281 ± 10	0.63 ± 0.17	3.56 ± 1.5	−6 ± 2
31.0	926 ± 20	0.27 ± 0.17	2.28 ± 0.28	6.3 ± 1.7
44.0	1928 ± 20	1.85 ± 0.64	3.02 ± 0.19	6.44 ± 0.74
62.0	3710 ± 23	3.56 ± 1.5	3.21 ± 0.22	5.6 ± 0.45
80.0	5540 ± 50	2.61 ± 0.95	2.97 ± 0.19	5.7 ± 0.5
		$P = 19$ bar		
31.0	205 ± 16	7.8 ± 10	4.5 ± 0.71	9.2 ± 0.4
44.0	429 ± 180	0.80 ± 1.00	3.2 ± 0.7	7.1 ± 3.2
62.0	890 ± 11	100 ± 85	4.4 ± 0.5	5.6 ± 0.7
80.0	1530 ± 13	5.2 ± 4.4	4.0 ± 0.4	6.0 ± 0.6
97.0	2200 ± 14	24 ± 26	4.8 ± 0.6	4.18 ± 0.33

(table 1) for 16, 17 and 19 bar are plotted in figure 8; these were then extrapolated linearly to lower pressures (full line) to obtain values of B where the dip in $\nu(T)$ was either very small or undetectable. The latter values were then used in fitting (4.4) to the data at the lower pressures. Some examples of fitted curves are compared with the data in figure 9.

Downloaded from rsta.royalsocietypublishing.org

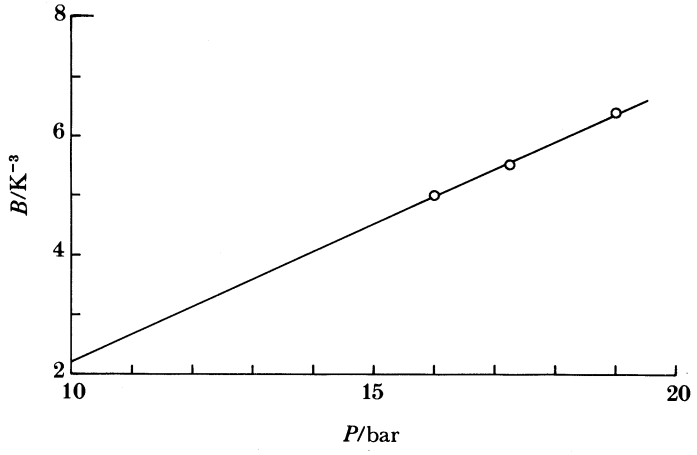

Figure 8. Values of the constant B obtained by fitting equation (4.4) to experimental data at three pressures. The line is drawn by eye through the points in order to extrapolate B to lower pressures.

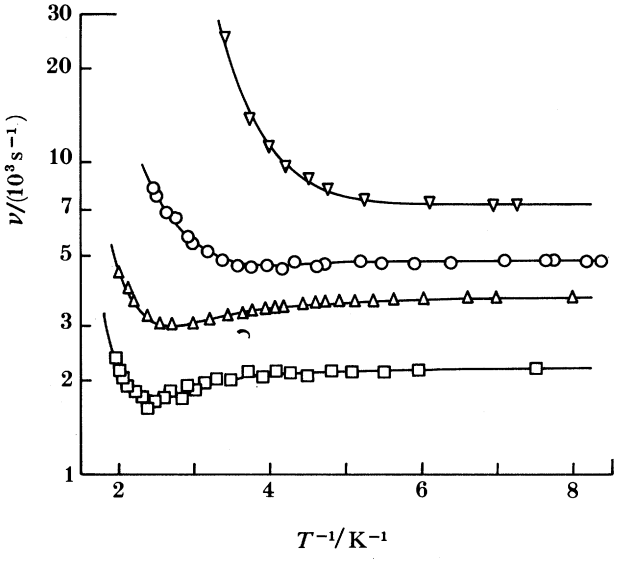

Figure 9. Some examples showing equation (4.4) fitted (full curves) to measured values of the vortex nucleation rate ν (points), plotted as a function of reciprocal temperature T^{-1}: ▽, $P = 12$ bar, $E = 1.77 \times 10^4$ V m^{-1}; ○, 15 bar 3.10×10^4 V m^{-1}; △, 17 bar, 6.20×10^4 V m^{-1}; □, 19 bar, 9.70×10^4 V m^{-1}. The parameter values used in generating the fitted curves are listed in table 1.

Fitted values of the parameters ν_0, A, E_b, and B obtained for various electric fields and pressures are listed in table 1. The barrier energy E_b appears to be roughly constant for each pressure and is almost independent of electric field for $E < 10^5$ V m^{-1}. There is one pressure (16 bar) for which we have analysed in detail at higher values of E, and these indicate that E_b decreases at higher fields when the ion travels faster. This result is in agreement with MVD, who showed that the barrier height decreases as the ionic velocity increases, as shown in figure 10.

In figure 11 we plot the average value of E_b, fitted for fields below 10^5 V m^{-1}, as a function of pressure. There appears to be a shallow minimum near 15 bar. The

Downloaded from rsta.royalsocietypublishing.org

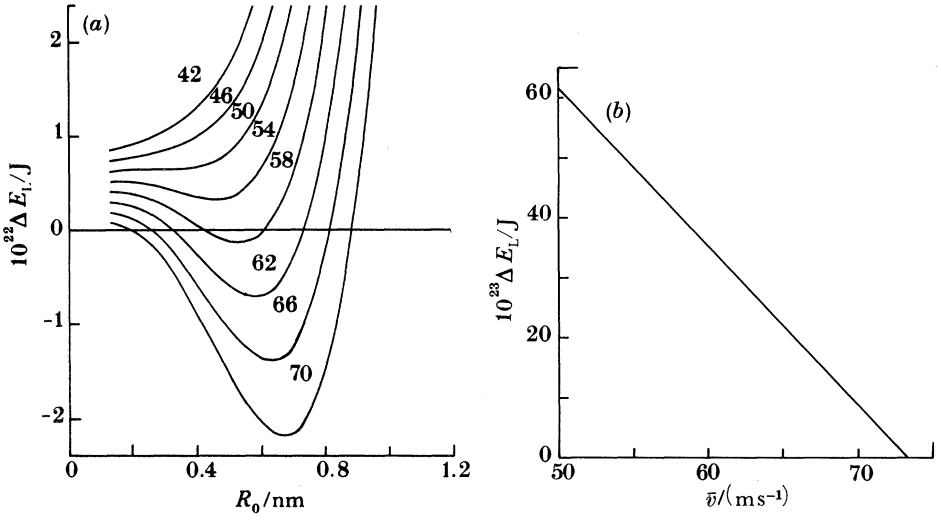

Figure 10. (*a*) The calculated change in energy ΔE_L that occurs in the MVD model when a vortex loop of radius R_0 is created at constant impulse in the equatorial plane of a negative ion travelling through He II at the velocities ($\mathrm{m\,s^{-1}}$) indicated by the numbers adjacent to the curves (after Muirhead *et al.* 1984). The MVD calculation cannot be extended to very small values of R_0, but it is expected that all the curves will pass through the origin. The energy barrier impeding vortex nucleation lies between the origin and the value of R_0 at which the curve first recrosses the $\Delta E_L = 0$ axis; the critical velocity for the process lies between 54 and 58 $\mathrm{m\,s^{-1}}$. The barrier height, to be associated with the parameter E_b extracted from the present experimental data, is therefore the height of the local maximum near $R_0 = 1$ Å. (*b*) The variation of ΔE_L with velocity v, interpolated from the curves of (*a*). It is to be expected that, except in very strong electric fields, the effective barrier height will be only slightly greater than the value corresponding to the critical velocity.

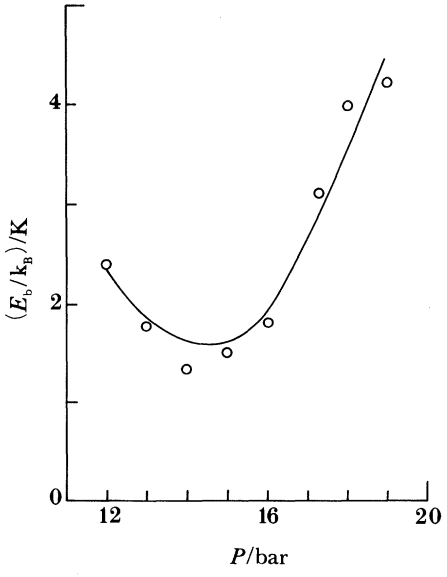

Figure 11. The energy barrier height E_b deduced by fitting equation (4.4) to the experimental $\nu(T)$ data, plotted as a function of pressure P. The curve is a guide to the eye.

Downloaded from rsta.royalsocietypublishing.org

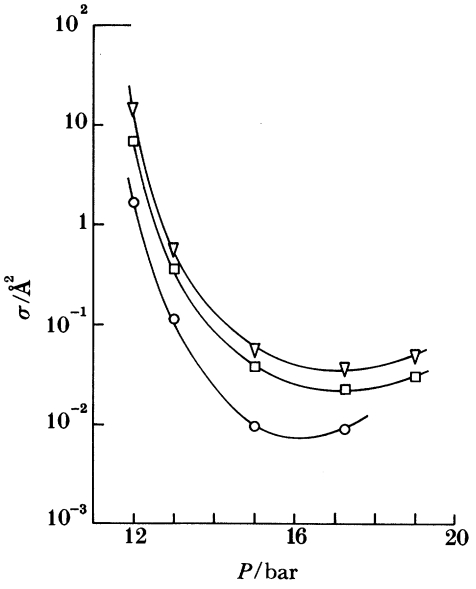

Figure 12. The cross section σ for the phonon assisted nucleation process, deduced from equation (4.3) after fitting equation (4.4) to the experimental data, as a function of pressure P, for three electric fields E: ○, 8.80×10^3 V m^{-1}; □, 4.40×10^4 V m^{-1}; ▽, 8.00×10^4 V m^{-1}. The curves are guides to the eye. Possible explanations for the strong pressure dependence of σ are discussed in the text.

existence of this minimum depends on the values of E_b at 12 and 13 bar, both of which are quite reliable. The minimum therefore appears to be a real, albeit somewhat puzzling, observation. It was not predicted by MVD. For pressures above 15 bar, E_b clearly increases quite rapidly with pressure. Eventually, E_b will become comparable with the roton energy gap of $\Delta/k_B \approx 7.5$ K, at a pressure of *ca.* 22 bar, and it then becomes impossible to separate the phonon and roton-assisted nucleation processes. In analysing the data, we have in fact restricted ourselves to temperatures below 0.5 K, so that there are very few thermal rotons present and we can ignore roton-assisted nucleation.

Now that we have determined the average value of the energy barrier E_b, we can use equation (4.3) to estimate the effective cross-section σ for the phonon-assisted nucleation process. In doing so, we first re-fit (4.4) to the data by using smoothed values of both E_b and B. The advantages of this procedure is that it minimizes the scatter in the values of σ and allows us to observe underlying trends in the variation of σ with E and P. The results are plotted as $\sigma(P)$ curves for fixed values of E in figure 12. The largest cross-section is *ca.* 15 Å^2, which is very much less than the geometrical cross-section of the ion (*ca.* 500 Å^2).

For any given pressure, σ increases with electric field. This arises in part from the presence of a critical velocity for the formation of a vortex: only ions travelling faster than this velocity will be able to produce vortex loops, even with phonon assistance, and the fraction of ions satisfying the condition will increase as the electric field is increased. This effect will be analysed later (see §4*e* below) after we have made an estimate of the critical velocity.

Another, even more striking, feature of figure 12 is the very rapid decrease in σ with increasing pressure near 12 bar.

Downloaded from rsta.royalsocietypublishing.org

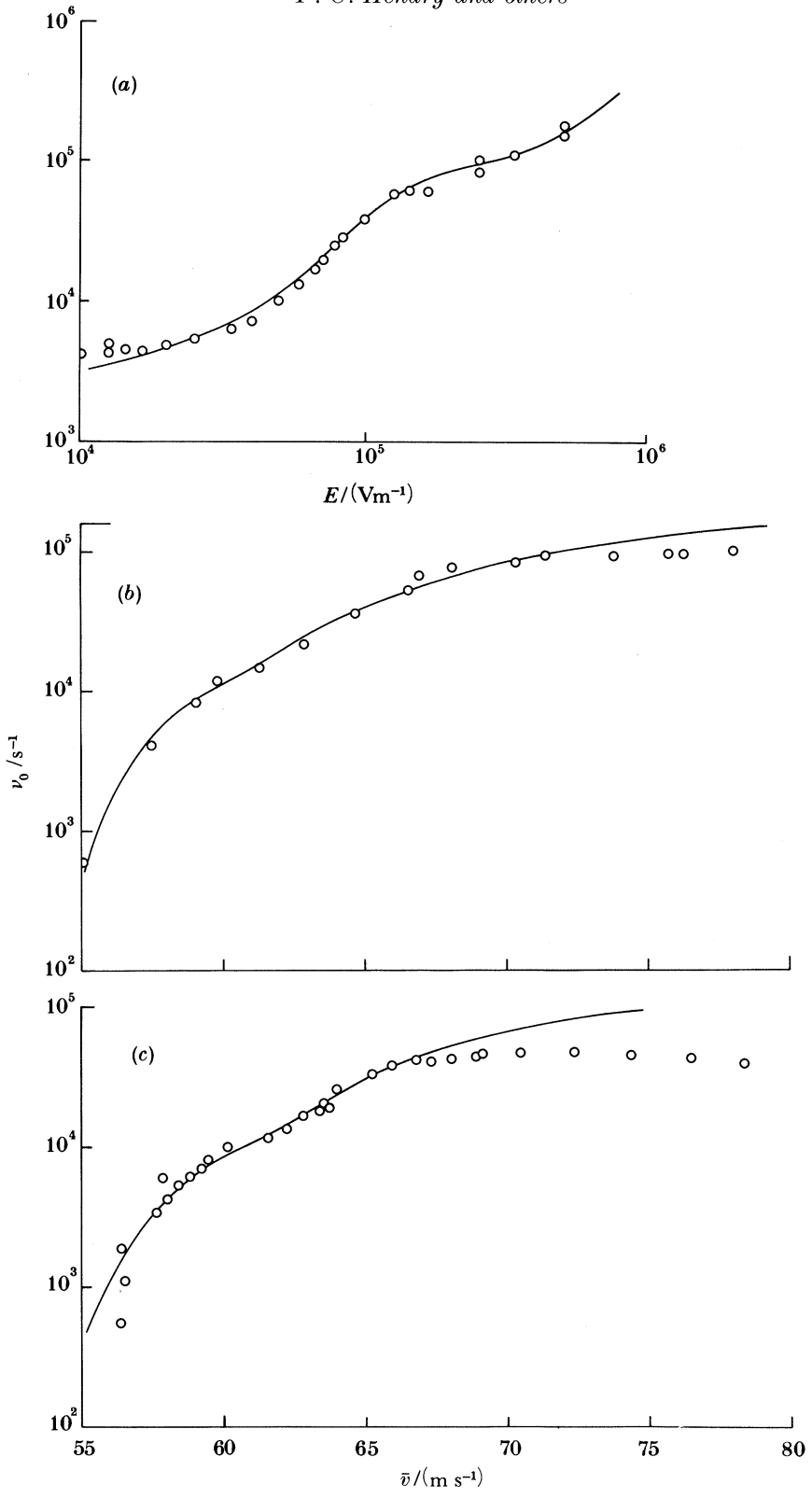

Figure 13*a*–*c*. For description see opposite.

PHILOSOPHICAL TRANSACTIONS OF THE ROYAL SOCIETY A MATHEMATICAL, PHYSICAL & ENGINEERING SCIENCES

PHILOSOPHICAL TRANSACTIONS OF THE ROYAL SOCIETY A MATHEMATICAL, PHYSICAL & ENGINEERING SCIENCES

Downloaded from rsta.royalsocietypublishing.org

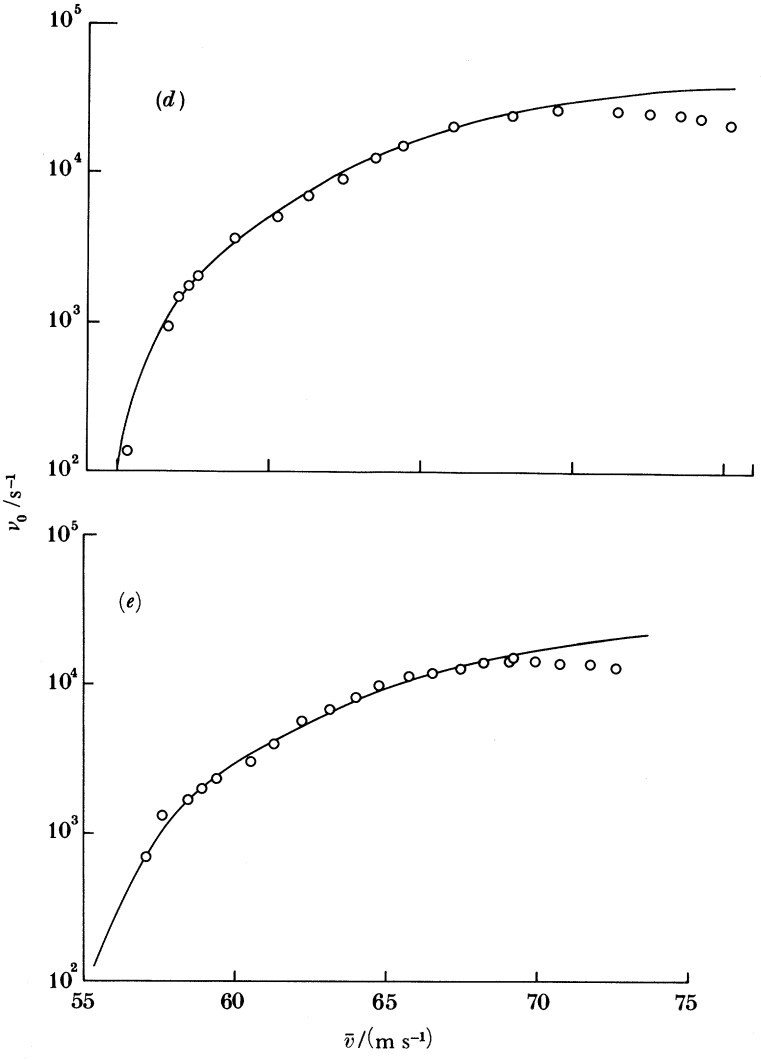

Figure 13. The velocity/electric field dependence of ν_0, the temperature-independent vortex nucleation rate extracted by fitting equation (4.4) to the experimental data: (*a*) $P = 13$ bar; (*b*) 15 bar; (*c*) 17 bar; (*d*) 19 bar; (*e*) 21 bar. The results are plotted as a function of ionic drift velocity $\bar{v}$, except in the case of the 13 bar data where a full set of velocity data is not available on account of the very large nucleation rate. The curves represent fits of equation (4.10) to the data; the corresponding parameter values are listed in table 2.

(*d*) *Electric field dependence of the tunnelling rate*

We now turn from the phonon-assisted nucleation process to the tunnelling process described by the first term of equation (4.4). The variation of $\nu_0(E)$ with electric field is shown in figure 3. For all pressures, ν_0 increases with E up to *ca.* 10^6 V m^{-1}, and then decreases again; similar behaviour was also found at higher pressures (see III). As already remarked above, an interesting feature of the data is the slight change in the slope of $\nu_0(E)$ that occurs near 10^5 V m^{-1}. The effect was just visible in the 19 bar data reported in III; at 13 bar it is very pronounced.

Downloaded from rsta.royalsocietypublishing.org

According to MVD, there is a critical velocity v_v above which vortex loops can be formed with conservation of energy and impulse. Whether or not the system then produces vortices at an observable rate depends on how rapidly it can tunnel through the potential barrier. As the velocity of the ion increases above v_v, the rate of production of vortices is expected by MVD to increase very rapidly. The simplest way to treat the system theoretically, as discussed in III, is to suppose that there is an effective critical velocity for vortex nucleation v_{v1} and that, for velocities $v > v_{v1}$, vortices are nucleated at a constant rate R_1. Thus the instantaneous production rate $R(v)$ will vary with velocity as

$$R(v) = R_1\,\theta(v - v_{v1}) \tag{4.5}$$

and the observed nucleation rate will be

$$\nu_0(E) = \int_0^\infty \mathrm{d}v\, f(v, E)\, R(v), \tag{4.6}$$

where $f(v, E)$ is the normalized distribution function of ionic velocities v in the electric field E. For low fields, it can be shown (Bowley & Sheard 1977) that

$$f(v, E) = \frac{1}{\Delta v}\exp\left[\frac{-\alpha m^*(v - v')^3}{3eE}\right] \tag{4.7}$$

so that the nucleation rate is expected (Bowley 1977) to vary as

$$\nu_0 \sim \exp\left[\frac{-\alpha m^*(v_{v1} - v')^3}{3eE}\right]. \tag{4.8}$$

Here v' is the critical velocity for roton pair emission by the ion which, as discussed in I, occurs at a rate $\alpha(v - v')^2$, and m^* is the effective mass of the ion. We expect ν_0 to increase as the field increases. As the pressure increases, so $(v - v')^2$ increases and causes ν_0 to decrease. These observations are in agreement with what is found experimentally.

By taking $R(v)$ to be of this simple form we can obtain an estimate of v_{v1}, the velocity at which vortex nucleation starts to occur at an appreciable rate. This velocity will be somewhat larger than the true critical velocity v_v.

We can make a quantitative comparison of experiment and theory by first calculating the distribution function using the method of Bowley & Sheard (1977), and then using it to calculate both the nucleation rate ν_0, from equation (4.6) and the drift velocity $\bar{v}$ from

$$\bar{v} = \int_0^\infty \mathrm{d}v\, v f(v, E). \tag{4.9}$$

To carry out this procedure, we require values of the Landau critical velocity v_L (see V), the effective mass of the ion (Ellis *et al.* 1983) and the roton momentum (Brooks & Donnelly 1977), all of which are known accurately. The calculated $\bar{v}$ and ν can then be compared with the experimental values. The greatest source of error comes from the measurement of the length of the induction space. To avoid this problem, the system was calibrated by requiring a plot of $\bar{v}(E^{\frac{1}{3}})$ to have the correct intercept v_L as previously measured in V, using a long time-of-flight chamber. The necessary adjustment was determined by fitting $\bar{v}(E)$ at 17.25 bar; for the nominally 11.3 mm cell a reduction of 2.9% was required in its directly measured length. Once

Downloaded from rsta.royalsocietypublishing.org

Table 2. *Values of parameters obtained by fitting equation* (4.10) *to the* $\nu(E)$ *data measured in the temperature-independent limit below 140* mK

P/bar	$R_1/(10^3\ \mathrm{s}^{-1})$	$R_2/(10^3\ \mathrm{s}^{-1})$	$v_{v1}/(\mathrm{m\ s}^{-1})$	$v_{v2}/(\mathrm{m\ s}^{-1})$
13	29	760	61	82
15	34	280	58	76
16	28	190	58	75
17	23	220	58	76
19	20	77	60	76
21	10	48	60	76

this calibration had been completed, the theory was fitted to the $\nu_0(v)$ data by adjusting R, v_{v1}, so as to obtain agreement.

At low pressure, where the nucleation rate in high fields becomes very large, the signal decays so rapidly that the right-hand side of the induction pulse is not well defined, as already mentioned above, and $\bar{v}$ cannot reliably be deduced from the data. What we have done in such cases is to fit the $\bar{v}(E)$ data in low fields, where ν is smaller and the measurements are therefore reliable, with the theory of Bowley & Sheard (1977). Once the theory had been fitted, values of $\bar{v}(E)$ at higher fields could be calculated. This technique was needed for the 13 bar results; the fitted values of R, and v_{v1} are likely to be less accurate as a result.

Regardless of the details of the fitting procedures, the simple form of equation (4.5) is unable to account for the increase in the slope of $\nu(E)$ near 10^5 V m^{-1}. As discussed earlier in III, this effect appears to imply the onset of a new vortex nucleation process at an appreciable rate when the ions travel at sufficiently high velocities. The data can be accounted for by adding an additional term to (4.5) to allow for the second nucleation mechanism,

$$R(v) = R_1\,\theta(v-v_{v1})+R_2\,\theta(v-v_{v2}). \tag{4.10}$$

The effect of the second critical velocity v_{v2} is to enable the theoretical $\nu_0(E)$ to increase more rapidly when $v > v_{v2}$.

The results of fitting (4.6) and (4.10) to the $\nu_0(E)$ data for pressures between 13 and 21 bar are shown by the curves in figure 13. The fits obtained are quite good, except for velocities above 70–72 m s^{-1} where the data below the fitted curve for all pressures. The latter effect is a precursor of the sharp drop in $\nu_0(E)$ that occurs for fields above 10^6 V m^{-1}: as discussed in III, it can be parameterized by the introduction of a third critical velocity v_{v3} at which $R(v)$ falls to zero; the present investigations concentrate on the region below the maximum in $\nu(E)$, however, and we have therefore felt it preferable to fit the data with (4.10) rather than to introduce an additional adjustable parameter. The fitted values of v_{v1}, v_{v2}, R_1 and R_2 are listed in table 2. They differ slightly, in the regions of overlap, from those reported in III. This is mainly because of the different form taken for $R(v)$, i.e. use of (4.10) in place of equation (50) of III.

Values of v_{v1} and v_{v2} are plotted as a function of pressure in figure 14. Also shown, for comparison, are values of the critical velocity v' for roton emission. Whereas v' decreases with increasing pressure, we find that v_{v1} remains approximately constant. Consequently, the quantity $(v_{v1}-v')$ increases with increasing pressure. It should be emphasized that the precise values of the fitted parameters are model-dependent and that, in using (4.10), we have taken a particularly simple and perhaps not very

Downloaded from rsta.royalsocietypublishing.org

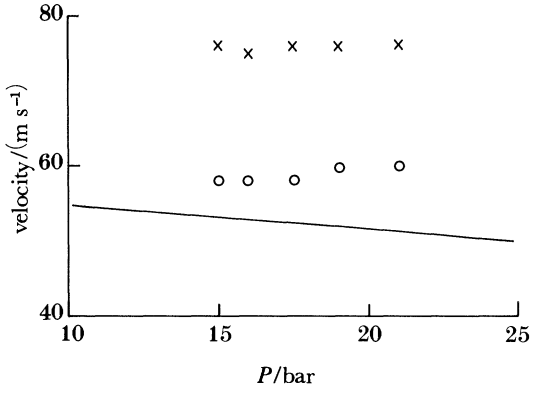

Figure 14. Pressure dependence of the critical velocities: ○, the first critical velocity for vortex nucleation v_{v1}, obtained by fitting equation (4.10) to the $\nu_0(E)$ data of figure 4.9; ×, values of the second critical velocity, v_{v2} identified with creation of a vortex loop in its first excited state, obtained by the same method. For comparison, the critical velocity for roton pair emission (see I) from the ion is shown by the curve: the experimental technique used for measurement of ν can be used only when $v_{v1} > v'$.

realistic model of the nucleation process; nonetheless the underlying trends, such as the dependence on pressure and the large difference between v_{v1} and v_{v2}, should be reliable.

In particular, we conclude that the additional vortex nucleation process whose onset occurs at v_{v2}, corresponding to the kinks in the measured $\nu_0(E)$ near 10^5 V m^{-1}, is a real effect that requires an explanation. It can, in fact, be accounted for quite plausibly within the framework developed by MVD. They propose that the vortex loop should be regarded as a quantum object which can tunnel through a potential barrier when it is energetically possible. The point out that a vortex in two dimensions can be treated as analogous to a charged particle in crossed electric and magnetic fields, the charge corresponding to the circulation κ of the vortex. When quantized, the vortex can exist in different 'Landau levels' separated by the cyclotron frequency

$$\omega_c = \kappa/\pi a^2. \tag{4.11}$$

Here, the vortex mass per unit length $m = \pi\rho a^2$, and a can be thought of as the radius of the vortex core if it were hollow. Now consider a thin film of thickness d. The mass of a vortex in the film will be md and the 'potential energy' also increases linearly with d. The cyclotron frequency will therefore be independent of d and so we will obtain the same set of quantized energy levels, i.e. we can extend the MVD idea to three-dimensional systems.

We propose that the vortex loop behaves much like the vortex in a film, despite the more complicated geometry. The curvature of the loop will of course change the potential energy but, provided this is a relatively small effect, we should still find that the separation of the energy levels is well approximated by $\hbar\kappa/\pi a^2$. The first critical velocity v_{v1} corresponds to tunnelling into the ground state; it seems reasonable to suppose that the second critical velocity v_{v2} corresponds to tunnelling into the first excited state. For the latter process to occur, the energy of the ion must be larger by about $\hbar\omega_c$ than that needed for ground state tunnelling, so that

$$\tfrac{1}{2}m^*(v_{v2}^2 - v_{v1}^2) \approx \hbar\omega_c = 2\hbar^2/m_4 a^2, \tag{4.12}$$

Downloaded from rsta.royalsocietypublishing.org

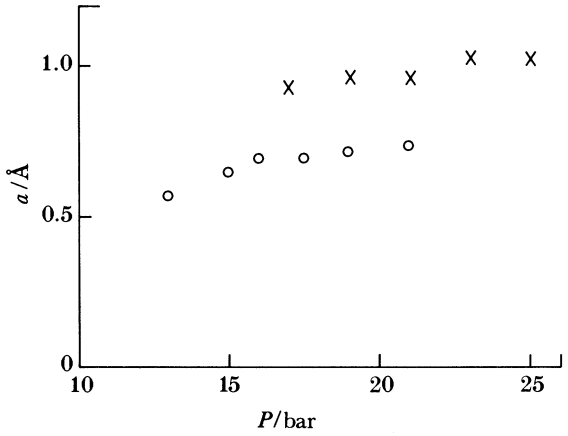

Figure 15. Values of the vortex core parameter a calculated from equation (4.10) using the fitted critical velocities v_{v1} and v_{v2} of figure 14 (circles), plotted as a function of pressure P. Values of a calculated in the same way from the critical velocities reported in III (crosses) differ slightly mainly because of the different form of $R(v)$ that was used.

where m_4 is the helium atomic mass and m^* is the effective mass of the ion. As a test of the model, we can use the fitted values of v_{v1} and v_{v2} (table 2 and figure 14) to estimate the size of the vortex core radius a, which is expected to be *ca.* 1 Å. Values of a deduced from (4.12) in this way are shown in figure 15, when the circles represent the present work and the crosses are derived from the values of v_{v1} and v_{v2} reported in III: as already noted, the latter differ slightly, mainly because of the different forms assumed for $R(v)$. In both cases, the deduced $a \approx 1$ Å, thus lending support to the hypothesis that the kinks in the data correspond to tunnelling into excited states. Typical values of $\hbar\omega_c/k_B$ are *ca.* 50 K, implying that thermal activation of these excited states of the vortex is virtually impossible.

What is the physical meaning of the excited states of a vortex loop? We may imagine the vortex loop to behave as a particle in the potential well $\Delta E_L(R_0)$ of figure 10*a*. If it were a classical object, the system would envolve continuously towards the minimum in the potential. However, we are here treating the vortex loop as a *quantum mechanical* object which can exist in a series of quantized energy states. The ground state energy of this level scheme corresponds to the local minimum in the potential $\Delta E_L(R_0)$ plus the zero point energy $\frac{1}{2}\hbar\omega_c$.

The other quantities that we obtain by fitting (4.10) to the $\nu_0(E)$ data are the two rate constants R_1 and R_2. Not very much can be concluded from R_2 because it is so sensitive to the fitted value of v_{v2} and because fitting the kinks in the data, given the random experimental errors in the latter, is subject to a measure of ambiguity. The fitted values of R_1, however, are more reliable and are of some interest. They are plotted as circles in figure 16*a*. Their variation with pressure is the inverse of that shown by $E_b(P)$ in figure 11: where E_b is minimum, R_1 is a maximum, and where $E_b(P)$ becomes large, R_1 becomes small. This is, of course, precisely the behaviour expected of a tunnelling object. The tunnelling rate should vary as

$$R_1 = \omega_0 \exp\left\{-2\int_0^R \mathrm{d}r\,[2md\,U(r)]^{\frac{1}{2}}/\hbar\right\}, \tag{4.13}$$

where md is the mass of the tunnelling loop and $U(r)$ represents the potential barrier,

Downloaded from rsta.royalsocietypublishing.org

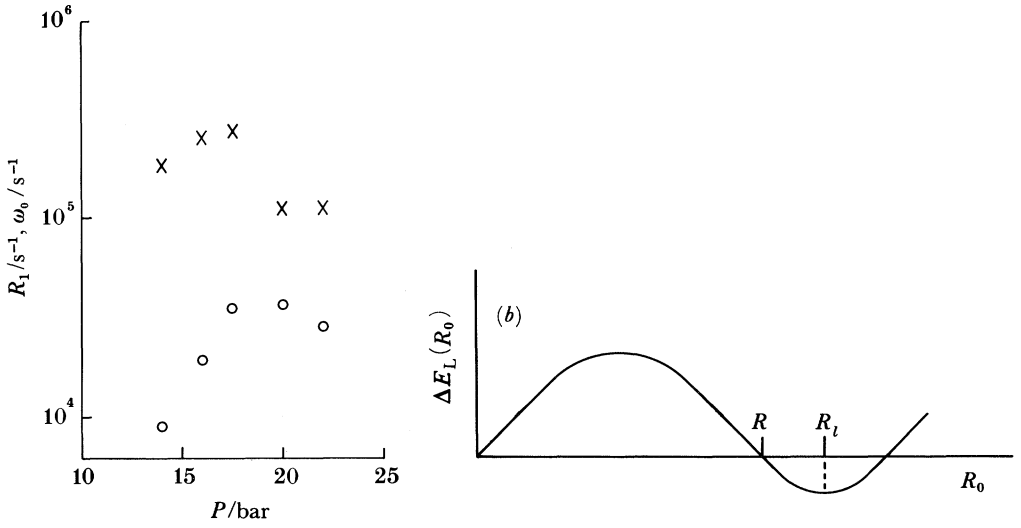

Figure 16. (*a*) Characteristic rates obtained by fitting equations (4.5), (4.6) and (4.10) to the experimental $\nu_0(E)$ data: ○, values of R_1; ×, estimates of ω_0 derived from the values of R_1 by use of equation (4.15). (*b*) Sketch of the energy barrier and potential minimum $\Delta E_L(R_0)$ to indicate the differences between the radii R, R_l and R_0.

which vanishes at $r = 0$ and $r = R$. The relationships between the radii R, R_l and R_0 are shown in figure 16*b*. (Recall that R_1 and R_2 are the rate constants defined by equation (4.10).) As the barrier increases, so R_1 is expected to decrease just as observed.

The detailed shape of the barrier is not known so, for convenience, we may parametrize it as

$$U(r) = \tfrac{27}{4}E_b\,(r/R)(1-r/R)^2 \tag{4.14}$$

so that the maximum of $U(r)$ is E_b. Then, if $d = \pi r$ so that the loop is semicircular, we find

$$\ln R_1 = \ln \omega_0 - (\pi R^{\frac{3}{2}} a/\hbar)(3\rho E_b/2)^{\frac{1}{2}}. \tag{4.15}$$

We already know the pressure dependences of ρ, a, E_b and R_1 so, on the assumption that the radius of the loop R_l is the independent of pressure and equal to *ca.* 5 Å, we can use (4.15) to estimate ω_0 as a function of pressure. The result is shown by the crosses in figure 16*a*, where, in deriving the 21 bar result, we estimated E_b at 21 bar as 6 K by extrapolation. Although the calculated values are subject to considerable scatter, it is evident that $\omega_0 \approx 2\times 10^5\ \mathrm{s}^{-1}$ and that it does not depend strongly on pressure.

(*e*) *The cross-section for phonon-driven vortex nucleation*

Now that we have deduced values for the critical velocity v_{v1}, we are in a position to discuss the electric field dependence of the cross section $\sigma(E)$ for phonon-assisted tunnelling. As already mentioned above in §4*c*, the simplest explanation of the increase in $\sigma(E)$ with field relates to the fact that only a fraction of the ions within the velocity distribution are able to nucleate vortices. In particular, only those whose velocities exceed v_{v1} can interact with phonons of energy greater than E_b to produce vortices; and this fraction rises with increasing E. If we assume that the cross section

Downloaded from rsta.royalsocietypublishing.org

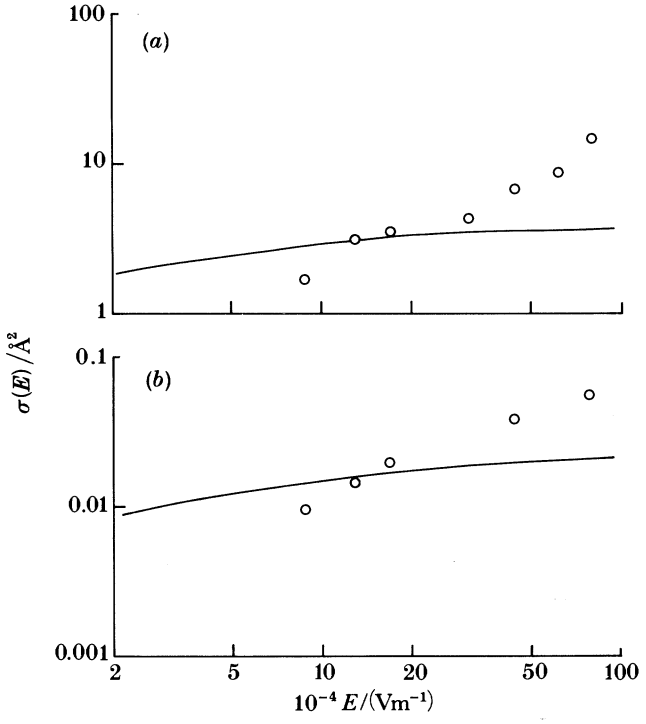

Figure 17. The cross-section σ for the phonon assisted nucleation process, deduced from equation (4.3) after fitting equation (4.4) to the experimental data, plotted (points) as a function of electric field E for two pressures: (*a*) $P = 12$ bar; (*b*) 15 bar. The curves represent the field variation of σ that would be expected to occur because of the increase with E of the fraction of ions travelling faster than v_{v1}. It is evident that the latter effect is not sufficient to account for the field dependence of σ.

σ_0 per ion in this high velocity group is constant, the effective cross-section averaged over all the ions will be

$$\sigma(E) = \sigma_0 \int_{v_{v1}}^{\infty} \mathrm{d}v f(v, E). \tag{4.16}$$

Knowing v_{v1}, it is possible to evaluate the integral and hence to predict the variation of σ with E that would be expected on this basis, resulting in the curves for 12 and 15 bar plotted in figure 17*a* and *b*. In both cases, the experimental values of $\sigma(E)$ increase more rapidly with E than the theoretical curves. The simple explanation is thus insufficient, in itself, to account for the observations. There are several possible explanations, and we now discuss the more plausible of them. First, we have taken account only of v_{v1}, and ignored the possible effect of the second critical velocity: this would help to explain the discrepancy in high electric fields at 12 bar. Secondly, we have ignored the variation in E_b with velocity that is to be expected on the basis of the MVD model. Properly, of course, we should fit to the data an expression of the form

$$\nu_{ph} = \int_{v_{v1}}^{\infty} \mathrm{d}v f(v, E) \frac{k_B T}{2\pi\hbar^3 c^3} E_b^2(v) \exp(-E_b(v)/k_B T), \tag{4.17}$$

where $E_b(v)$ is a decreasing function of v for velocities above v_{v1}. Although we could

Downloaded from rsta.royalsocietypublishing.org

in principle analyse the data using such a model, their precision is not sufficient to make the exercise likely to be fruitful, particularly given that an upper critical velocity for phonon assisted nucleation should also be taken into account.

We can, however, draw one important conclusion, namely, that the sudden and dramatic decrease in σ_0 with pressure between 12 and 15 bar is a real effect. It cannot be accounted for in terms of a reduction with increased pressure in the fraction of ions travelling faster than v_{v1}. In the range of electric fields studied, this fraction changes by a factor of *ca.* 3 whereas, in contrast, σ_0 changes by nearly two orders of magnitude.

5. Conclusion

The main conclusions emerging from the present work can be summarized as follows.

1. Vortex nucleation in He II is impeded by an energy barrier, vindicating an early suggestion by Vinen (1963).

2. Below 0.3 K, the nucleation mechanism involves a form of macroscopic quantum tunnelling through the barrier; at higher temperatures, thermally activated processes can also occur, kicking the system over the barrier.

3. The thermally activated process can be interpreted in terms of a phonon-assisted nucleation mechanism, exactly analogous to the roton assisted process at higher pressures discussed in III.

4. The barrier heights deduced from the experimental data are consistent with the calculations of MVD and their small magnitudes confirm the conclusion that the initial vortex is a tiny loop rather than a large encircling ring (contrary to the tentative conclusion reached in III).

5. The minima in some of the $\nu(T)$ curves, corresponding to a decrease of the tunnelling rate with increasing temperature, are apparently too deep to be accounted for simply in terms of the reduced ionic velocities caused by phonon scattering. An explanation is proposed in terms of a phonon damping mechanism that acts directly upon the tunnelling process.

6. The kinks in the low temperature $\nu(E)$ curves, corresponding to the onset of an additional nucleation mechanism, are attributed to tunnelling of the system into the first excited state of the nascent vortex loop.

The work has also led to some new and interesting questions, as well as to the re-opening of some older ones. In particular, we would like to know answers to the following:

1. Why does the barrier height E_b vary with pressure (figure 11) in such a dramatic way? There is nothing in the theory of MVD, or in the physics of negative ions, that would have led one to anticipate a rapid change in E_b near 15 bar. (We note that the rapid pressure variation of the roton pair emission matrix element over a similar pressure range, reported in V, also remains unexplained.)

2. What causes the spontaneous nucleation rate corresponding to the first critical velocity to be *ca.* $2\times10^5\ \mathrm{s}^{-1}$, a value that is much less than typical frequencies in He II and certainly much less than the cyclotron frequency, the natural frequency scale for the problem? Is the reduction caused by dissipation, perhaps the dissipation associated with the roton emission?

3. Why does the nucleation rate drop in high electric fields? This drop affects both the spontaneous and the thermally activated nucleation rates. It could be associated either with the increase in dissipation with the velocity of the ion, or, as suggested

Downloaded from rsta.royalsocietypublishing.org

in III, with a tendency of the ion to evade capture by the nascent vortex or, equivalently, with an instability of the initial ion–ring complex in very strong electric fields.

4. What causes the rapid pressure variation of the cross section for the phonon assisted nucleation process (figure 12)? It is this effect which gives rise to the disappearance of the dip in $\nu(T)$ as the pressure is reduced.

Finally, we would remark that, although the present investigation has related to the special (very well characterized) case of vortex formation by moving negative ions, we anticipate that the main features of the results should be of much wider relevance. In particular, we expect that our central conclusion, that the process involves macroscopic quantum tunnelling through a small energy barrier, should be quite generally applicable to vortex creation in He II.

It is a pleasure to acknowledge valuable discussions and correspondence about various aspects of the work with P. Hanggi, R. Mannella, W. F. Vinen and E. Varoquaux. The research was supported by the Science and Engineering Research Council to whom two of us (P.C.H. and C.D.H.W.) are also grateful for the support, respectively, of a Studentship and a Research Associateship.

References

Allum, D. R., McClintock, P. V. E., Philips, A. & Bowley, R. M. 1977 *Phil. Trans. R. Soc. Lond.* A **284**, 179–224. (Referred to in text as I.)

Avenel, O. & Varoquaux, E. 1985 *Phys. Rev. Lett.* **55**, 2704–2707.

Avenel, O. & Varoquaux, E. 1987 *Phys. Rev. Lett.* **59**, 1168.

Awschalom, D. D. & Schwarz, K. W. 1984 *Phys. Rev. Lett.* **52**, 49–52.

Beecken, B. P. & Zimmermann, W. 1987 *Phys. Rev.* B **35**, 1630–1635.

Bowley, R. M. 1976 *J. Phys.* C **9**, L367–370.

Bowley, R. M. 1984 *J. Phys.* C **17**, 595–613.

Bowley, R. M., McClintock, P. V. E., Moss, F. E., Nancolas, G. G. & Stamp, P. C. E. 1982 *Phil. Trans. R. Soc. Lond.* A **307**, 201–260. (Referred to in text as III.)

Bowley, R. M. & Sheard, F. W. 1977 *Phys. Rev.* B **16**, 244–254.

Brooks, J. S. & Donnelly, R. J. 1977 *J. Phys. Chem. Ref. Data* **6**, 51–104.

Caldeira, A. O. & Leggett, A. J. 1983 *Ann. Phys.* **149**, 374–456.

Ellis, T. & McClintock, P. V. E. 1985 *Phil. Trans. R. Soc. Lond.* A **315**, 259–300. (Referred to in text as V.)

Ellis, T., McClintock, P. V. E. & Bowley, R. M. 1983 *J. Phys.* **16**, L485–489.

Ellis, T., McClintock, P. V. E., Bowley, R. M. & Allum, D. R. 1980 *Phil. Trans. R. Soc. Lond.* A **296**, 581–595. (Referred to in text as II.)

Fetter, A. L. 1964 *Phys. Rev.* A **136**, 1488.

Hendry, P. C., Lawson, N. S., McClintock, P. V. E., Williams, C. D. H. & Bowley, R. M. 1988 *Phys. Rev. Lett.* **60**, 604–607.

Hendry, P. C., Lawson, N. S., Williams, C. D. H., McClintock, P. V. E. & Bowley, R. M. 1987 *Japanese J. appl. Phys. Suppl.* **26**(3), 73–74.

Hendry, P. C., Lawson, N. S., Williams, C. D. H., McClintock, P. V. E. & Bowley, R. M. 1989 In *Elementary excitations in quantum fluids* (ed. K. Ohbayashi & M. Watabe), pp. 184–188. Heidelberg.

Hendry, P. C. & McClintock, P. V. E. 1987 *Cryogenics* **27**, 131–138.

Hess, G. B. 1971 *Phys. Rev. Lett.* **27**, 977–979.

Muirhead, C. M., Vinen, W. F. & Donnelly, R. J. 1984 *Phil. Trans. R. Soc. Lond.* A **311**, 433–467. (Referred to in text as MVD.)

Nancolas, G. G., Bowley, R. M. & McClintock, P. V. E. 1985 *Phil. Trans. R. Soc. Lond.* A **313**, 537–606. (Referred to in text in IV.)

PHILOSOPHICAL TRANSACTIONS OF THE ROYAL SOCIETY A MATHEMATICAL, PHYSICAL & ENGINEERING SCIENCES

PHILOSOPHICAL TRANSACTIONS OF THE ROYAL SOCIETY A MATHEMATICAL, PHYSICAL & ENGINEERING SCIENCES

Downloaded from rsta.royalsocietypublishing.org

Pines, D. 1966 *Quantum fluids* (ed. D. D. Brewer), p. 328. New York: Wiley.

Rayfield, G. W. 1966 *Phys. Rev. Lett.* **16**, 934–936.

Schwarz, K. W. 1987 *Phys. Rev. Lett.* **59**, 1167.

Schwarz, K. W. & Jang, P. S. 1973 *Phys. Rev.* A **8**, 3199–3210.

Tough, T. J. 1982 In *Progress in low temperature physics* (ed. D. F. Brewer), vol. VIII, ch. 3. Amsterdam: North-Holland.

Varoquaux, E., Meisel, M. W. & Avenel, O. 1986 *Phys. Rev. Lett.* **57**, 2291–2294.

Vinen, W. F. 1963 In *Liquid Helium Proc. Int. School of Physics, Enrico Fermi, course XXI* (ed. G. Careri), p. 336. New York: Academic Press.

Received 8 March 1990; accepted 6 April 1990

PHILOSOPHICAL TRANSACTIONS OF THE ROYAL SOCIETY A MATHEMATICAL, PHYSICAL & ENGINEERING SCIENCES

PHILOSOPHICAL TRANSACTIONS OF THE ROYAL SOCIETY A MATHEMATICAL, PHYSICAL & ENGINEERING SCIENCES